Scripta Materialia 188 (2020) 233–237

Contents lists available at ScienceDirect

Scripta Materialia

journal homepage: www.elsevier.com/locate/scriptamat

# Magnetic contributions in multiferroic gadolinium modified bismuth ferrite ceramics

Julian Walker[a,*], Anja Mirjanic[b,c], Uros Prah[b,c], Matej Sadl[b,c], Oana Andreea Condurache[b,c], Andreja Bencan[b,c], Tadej Rojac[b,c], Marian Grigoras[d], Hana Ursic[b,c]

[a] Department of Materials Science and Engineering, Norwegian University of Science and Technology, Trondheim, Norway
[b] Electronic Ceramics Department, Jozef Stefan Institute, Ljubljana, Slovenia
[c] Jozef Stefan International Postgraduate School, Ljubljana, Slovenia
[d] National Institute of Research and Development for Technical Physics, Iasi, Romania

ARTICLE INFO

*Article history:*
Received 27 May 2020
Accepted 20 July 2020
Available online 29 July 2020

*Keywords:*
Multiferroics
Ceramics
rare earth modified $BiFeO_3$
Secondary phases

ABSTRACT

$Bi_{0.88}Gd_{0.12}FeO_3$ multiferroics are of interest for next-generation electronics and are shown with a remnant magnetization 0.2 emu·g$^{-1}$, coercive field 8 kOe, Curie temperature 370 °C and magnetization of 0.7 emu·g$^{-1}$ at magnetic fields 30 kOe. Scanning probe microscopy confirmed the intrinsic multiferroicity in the perovskite phase with coexistence of ferroelectric/ferroelastic and ferromagnetic domain structures. Strong magnetic hysteresis was produced by thermal cycling to 1000 °C due to degeneration of the perovskite phase into iron oxide inclusions, highlighting the importance of processing, thermal history and thermodynamic stability for minimizing the amount of parasitic magnetic secondary phases.



Multiferroics promise functionality useful for spintronics and applications like low-energy, high-density memory [1]. For more than two decades, bismuth ferrite (BFO) has been a central material for fundamental multiferroics research, primarily because its intrinsic multiferroicity at room temperature (RT), ferroelectric polarization along the $[111]_{pc}$ (pc denoting pseudocubic) with a Curie temperature of 820 °C coexisting with a G-type antiferromagnetic order with a Néel temperature of 370 °C [2,3,4]. While the ferroelectric polarization of bismuth ferrite is promising, with remanent polarization up to 100 μC·cm$^{-2}$ in thin films and single crystals [5,6], the antiferromagnetic response is problematic due to its effectively zero remanent and weak magnetization, <0.4 emu·g$^{-1}$ at magnetic fields of 60 kOe [7]. As a result, breaking the antiferromagnetic ordering and increasing the total magnetic susceptibility of BFO without destroying the multiferroicity is an important area of research.

The antiferromagnetic response of BFO arises from the approximate antiparallel ordering of the neighboring $Fe^{3+}$ spins due to super exchange and a long range super structure of an incommensurate spin cycloid that propagates along $[110]_{pc}$ [4]. Breaking this antiferromagnetic ordering and increasing both the remanent magnetization and the magnetic susceptibility has been achieved by substitution of both the A and B-sites of the crystal lattice, using end member compositions, such as $BaTiO_3$, $SrTiO_3$ and $REFeO_3$, where RE is a rare earth element (e.g. La, Sm, Gd, Dy) [8,9,10]. Rare earth substitution is promising for magnetic properties due to the strong localized magnetic moments of these elements, caused by the partially filled inner electron shells seen by the *4f* electron configuration [2,11]. The rare earth modified BFO solid solutions have attracted attention because they can exhibit increased ferromagnetic response, larger piezoelectric coefficients, and reduced ferroelectric coercive fields ($E_c$) compared to the parent bismuth ferrite [10,12].

Characterization of the ferromagnetic properties of bismuth-ferrite-based solid solutions is nontrivial and has resulted in discrepancies among the literature. The chief cause of discrepancy originates from the tendency of bismuth-ferrite-based ceramics to segregate into bismuth-rich and iron-rich secondary phases during synthesis, which leads to debate over the origin of macroscopically measured magnetic properties [13,14,15]. The concern is that the macroscopic magnetic response often includes contributions from Fe-rich phases such as $\gamma$-$Fe_2O_3$, $Fe_3O_4$, and $Bi_2Fe_4O_9$-based spinel-like derivatives, as well as, or in lieu of, the matrix perovskite phase. Therefore, in many modified BFO compositions there remains some question over the magnetism of the perovskite matrix.

Here, we show the macroscopic magnetization of gadolinium-modified bismuth ferrite (with nominal composi-

* Corresponding author.
*E-mail address:* julian.walker@ntnu.no (J. Walker).

https://doi.org/10.1016/j.scriptamat.2020.07.045

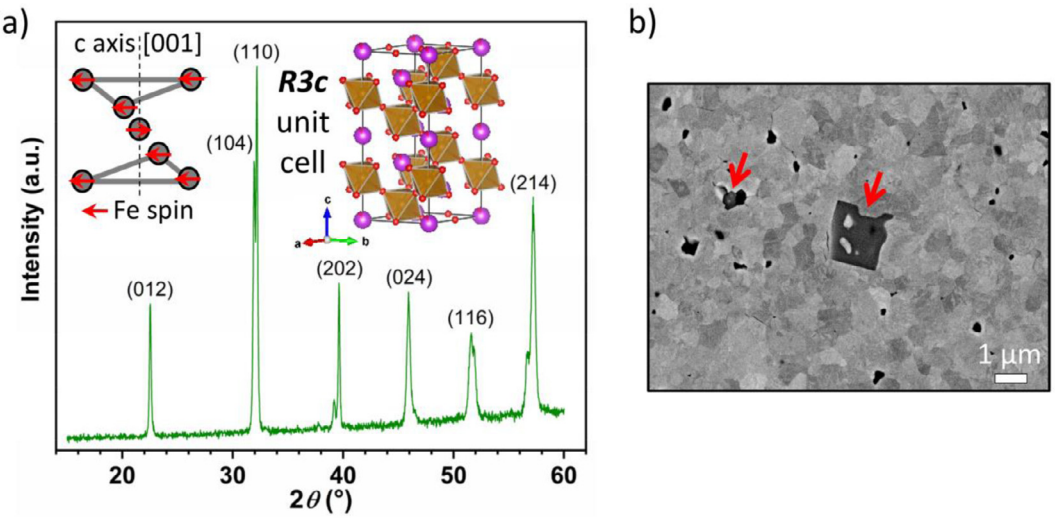


**Fig. 1.** a) Powder XRD pattern for $Bi_{0.88}Gd_{0.12}FeO_3$ with major peaks labelled according to the rhombohedral notation. Inset (left) shows the magnetic structure of the Fe spins of the R3c bismuth ferrite structure and the inset (right) shows the R3c structure derived from the data fit. b) SEM micrograph of polished ceramic surface with red arrows indicating Fe-rich secondary phase. Grain morphology and domain structure can be seen in greyscale contrast with black spots showing porosity.

tion $Bi_{0.88}Gd_{0.12}FeO_3$) demonstrating its ferrimagnetic properties on the bulk and the local level, the latter probed with magnetic force microscopy (MFM) of the ferrimagnetic domains present in the perovskite matrix phase and secondary phases. This study confirms the ferrimagnetic order of the perovskite matrix.

Ceramic pellets were prepared with a mechanochemical assisted synthesis method reported in detail elsewhere [16]. After 40 h of mechanochemical activation samples were milled in ethanol to break up agglomerates before being uniaxial pressed at 150 MPa and sintered for 3 h at 800 °C. Sintered pellets were crushed before powder X-ray diffraction measurements on at PANalytical X'Pert PRO (PANalytical, Almelo, Netherlands) high-resolution diffractometer ($CuK\alpha_1$ radiation) equipped with a 100 channel X'Celerator detector. Diffraction patterns were recorded in the 15–60° 2-Theta-range with a step of 0.017° and an integration time of 100 s per step at RT.

Sample surfaces were polished down to 0.25 µm with diamond paste followed by 6 h of silica gel polishing in dilute KOH solution. Surfaces prepared this way were used for scanning electron microscopy (SEM) with a field-emission scanning electron microscope (FE-SEM, JSM-7600F, Jeol Ltd., Tokyo, Japan) equipped with an energy dispersive X-ray spectrometer (EDXS, Inca Oxford 350 EDS SSD, Oxford Instruments, Abingdon, U.K.) and both piezo-response force microscopy (PFM) and MFM measurements with an Asylum Research, CA, USA, Molecular Force Probe 3D atomic force microscope. The PFM out-of-plane amplitude and phase images were measured in the dual AC resonance-tracking mode (frequency ~350 kHz). A tetrahedral Si tip coated with Ti/Ir (Asyelec-01, Atomic Force F&E GmbH, Germany) with a curvature diameter of ~20 nm was used. The MFM images were measured using the two-pass MFM technique, where MFM signal is derived from the variations in cantilever's resonance frequency (denoted as MFM frequency image) and phase of oscillation (denoted as MFM phase image) when the cantilever-tip system interacts with the stray magnetic fields above the sample [17]. Si tips coated with CoCr (ASYMFMHM, AtomicForce F&E GmbH, Germany) and Fe (ASYMFMLC, AtomicForce F&E GmbH, Germany) were used for MFM scanning experiments. First, the MFM tip was magnetized with the north pole of a permanent magnet, and for the second scan the MFM tip was magnetized with the south pole of a magnet. The reversal of the tip polarity resulted in the inversion of the MFM contrast, which revealed that the signal pattern observed was of magnetic origin. Prior to sample investigation, the MFM measurements were performed on a computer hard disk reference sample (Supplementary material, A). The temperature dependence of magnetic moment was measured in a temperature range from 25 to 1000 °C with a magnetic field of 10 kOe using a vibrating sample magnetometer (VSM, Lake Shore 7410, USA). The magnetization ($M$) values were obtained by normalizing the magnetic moment with the mass of the sample. The magnetization versus magnetic field ($M$–$H$) hysteresis loop was measured in magnetic fields up to 30 kOe at RT.

We begin by showing the structure and microstructure of the analyzed ceramics. The prepared ceramics had a majority rhombohedral *R3c* phase (Fig. 1a). All XRD peaks were identified by the *R3c* structure, with the magnetic structure and unit cell according to the schematic and model given in the inset of Fig. 1a. It is possible that the matrix phase consists of small fractions (<10 wt%) of antiferroelectric *Pbam* phase as reported in the literature, but due to peak overlapping the presence of this phase could not be distinguished with greater accuracy [16]. Traces of *Pbam* were found in the ceramics using transmission electron microscopy in previous studies [18].

While no secondary phases were detectable in the XRD patterns, SEM-EDXS was used to establish the presence of secondary phases (Fig. 1b). The SEM micrograph of polished ceramic surface shows a dark, Fe-rich, rectangular phase region (marked with red arrows) embedded in the Gd-doped BFO matrix phase. The rectangular morphology of the Fe-rich phase was consistent with the $Bi_2Fe_4O_9$-based phase typically observed in $BiFeO_3$ ceramics [19]. Brighter inclusions in the Fe-rich phase could be Bi-rich (sillenite) phase or BFO matrix (for details see supplementary material B). The Bi-rich sillenite phase that is commonly found in bismuth-ferrite-based ceramics was also observed in small quantities at triple points and grain boundaries, where it is typically found due to its low melting point <500 °C [14,19]. Within the matrix, small, irregularly shaped black areas were identified as pores.

The rare earth substitution for $Bi^{3+}$ at the A-site of the perovskite was proposed to break the G-type antiferromagnetism by suppression of the spiral spin modulation of the $Fe^{3+}$ in unmodified bismuth ferrite [10,20,21]. By changing the super exchange interaction through distortion of the O-Fe-O bond angle the $Gd^{3+}$ substitution in $Bi_{0.88}Gd_{0.12}FeO_3$ resulted in weak ferrimagnetic properties.

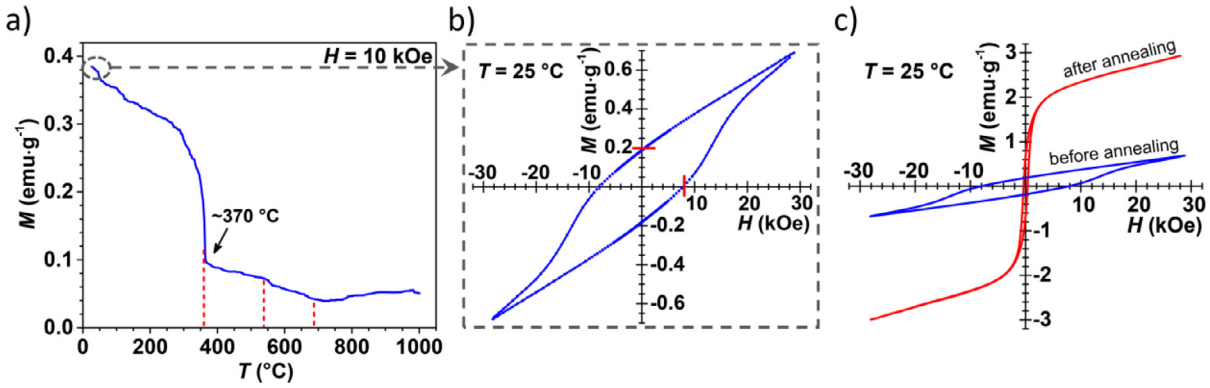


**Fig. 2.** Magnetization (M) of $Bi_{0.88}Gd_{0.12}FeO_3$. a) Temperature dependence of M measured at 10 kOe. b) M–H hysteresis loop measured at 25 °C for $Bi_{0.88}Gd_{0.12}FeO_3$ before thermal excursion to 1000 °C. c) M–H hysteresis loop measured at 25 °C before (blue) and after (red) thermal excursion to 1000 °C.

Under a magnetic field of 10 kOe at RT the $M$ of $Bi_{0.88}Gd_{0.12}FeO_3$ was ~0.38 emu·g$^{-1}$ (Fig. 2a). $M$ decreased steadily to 0.28 emu·g$^{-1}$ at 250 °C then dropped to <0.10 emu·g$^{-1}$ between 300 and 370 °C. This drop was consistent with the known Néel temperature ($T_N$) of unmodified BFO [4]. From 370 to 700 °C $M$ remained above zero but declined further with a local maximum around 550 °C. A likely explanation for this is the presence of the Fe-rich phases, such as $Bi_2Fe_4O_9$-based spinel, $\gamma$-$Fe_2O_3$ and $Fe_3O_4$. Stoichiometric $Bi_2Fe_4O_9$ is typically paramagnetic above RT [22], but changes to the stoichiometry may alter its magnetization and Si impurity is particularly common in $BiFeO_3$ secondary phases, as seen in the EDXS (supplementary Fig. S2) [14,23]. $\gamma$-$Fe_2O_3$ and $Fe_3O_4$ are ferrimagnetic with magnetic Curie temperatures ($T_C$) of approximately 570 °C, which correlates with the temperature of a feature seen in Fig. 2a above the $T_C$ of the matrix perovskite phase (Fig. 2a) [18,24]. Between the temperature of 700 to 1000 °C the magnetic response increased marginally, likely the result of a change in the phase composition of the ceramics, such as an increase in the amount of Fe-rich secondary phase due to the volatility of $Bi^{3+}$ and the thermodynamic instability of the perovskite phase in this temperature range [15,19].

The $M$–$H$ hysteresis loop measured at RT (Fig. 2b), showed characteristics distinct from the antiferromagnetic response of the parent BFO where no remanent magnetization ($M_r$) occurs [7]. While the magnetization for $Bi_{0.88}Gd_{0.12}FeO_3$ was small, the hysteresis as a function of magnetic field clearly shows $M_r$ of 0.2 emu·g$^{-1}$, a saturated magnetization ($M_s$) of near 0.7 emu·g$^{-1}$ and coercive magnetic field ($H_c$) of 8 kOe, both marked by red in Fig. 2b. At magnetic fields >10 kOe the loop began to pinch together, narrowing at fields around 20 kOe in both positive and negative field directions, above which the magnetization moved towards a linear relationship with respect to magnetic field but did not reach a clear saturation. This $M$–$H$ loop shape was thought to be symptomatic of the superposition of two or more magnetic orders. Potentially the weak ferromagnetic order of the Gd substituted structure, a weak antiferromagnetic ordering residual from the parent $BiFeO_3$ structure, and ferromagnetic ordering from Fe-rich phases.

To confirm the effect of large amounts of Fe-rich phase, and subsequently the role of $Bi^{3+}$ volatization on the magnetic response of the material, a second $M$–$H$ measurement at RT was performed after the material had experience the thermal excursion to 1000 °C (Fig. 2c). After thermal excursion the ferromagnetic response significantly increased to a $M_r$ of 0.7 emu·g$^{-1}$, $M_s$ of nearly 3 emu·g$^{-1}$ and $H_c$ of 0.36 kOe. This behavior is explained by an increased presence of iron oxide phases, $\gamma$-$Fe_2O_3$ or $Fe_3O_4$, which can have $M_s$ on the order of 80 emu·g$^{-1}$ [24]. Using the $M_s$ of the ceramic before thermal excursion and the approximate $M_s$ of the iron oxides, the weight percentage of $\gamma$-$Fe_2O_3$ and $Fe_3O_4$ was estimated at less than 5 wt%. This demonstrates the huge effect that the presence of strong ferrimagnetic Fe-rich secondary phases can have on the magnetic response of $BiFeO_3$-based materials.

The drawback of macroscopic magnetic measurements, such as those in Fig. 2, are that they are unable to separate the responses of the matrix perovskite phase from that of any secondary phases present. MFM was used to confirm the magnetization on a submicrometer length scale by imaging the magnetic domain structure [25,26]. Local measurements were performed on a 40 × 40 μm section of the $Bi_{0.88}Gd_{0.12}FeO_3$ surface using an AFM (Fig. 3). gray-scale contrast derived from tip height and deflection measurements were used to identify a region containing a single grain with an inclusion of rectangular morphology identified as an Fe-rich phase (Fig. 3a and b, see blue square). The chemical composition was verified with EDXS point analysis (supplementary material, B). The piezoelectric response on the materials was measured using PFM and the images show a strong bright and dark contrast for the *R*3*c* matrix phase (Fig. 3c). The bright and dark contrast regions arise from the approximate up and down polarization directions of ferroelectric/ferroelastic domains that produce opposite piezoelectric responses to the electric voltage applied by the tip. The irregular ferroelectric/ferroelastic domain pattern was consistent with that reported previously for $Bi_{0.88}Gd_{0.12}FeO_3$ ceramics [18].

By contrast to the local piezoelectric response of the matrix, the rectangular inclusion, had no distinguishable domain contrast in the PFM mode (Fig. 3c). Higher spatial resolution images of this region (Fig. 3d-i), showed that the inclusion displayed different etching and polishing rates to the matrix, as observed by the height contrast image (Fig. 3d and e), but the signal of the inclusion in both amplitude (Fig. 3f) and phase (Fig. 3g) PFM images was zero. This confirmed that the rectangular inclusion was piezoelectrically inactive. This was expected as the phase morphology and composition is consistent with an $Bi_2Fe_4O_9$-based derivative, so it likely has an orthorhombic *Pbam* structure and is antiferroelectric with a center of symmetry over unit cell pairs [23].

The same area was then scanned using the magnetic tip and the MFM in frequency and phase mode, shown in Fig. 3h and i. In these MFM measurements the light and dark contrast corresponds to approximately oppositely oriented ferromagnetic domains with respect to the measured direction. The contrast is less pronounced for the magnetic domain structure with respect to the ferroelectric domains (compare Figs. 3f,g with Figs. 3h,i) but this is to be expected due to the small magnetic signal (i.e. <0.3 emu·g$^{-1}$) of these materials (refer to Fig. 2). The magnetic contrast in the frequency and phase measurements is visible in both the matrix and secondary phase, consistent with the idea that Fe-rich secondary phases contribute to the bulk magnetization of ceramic [13].

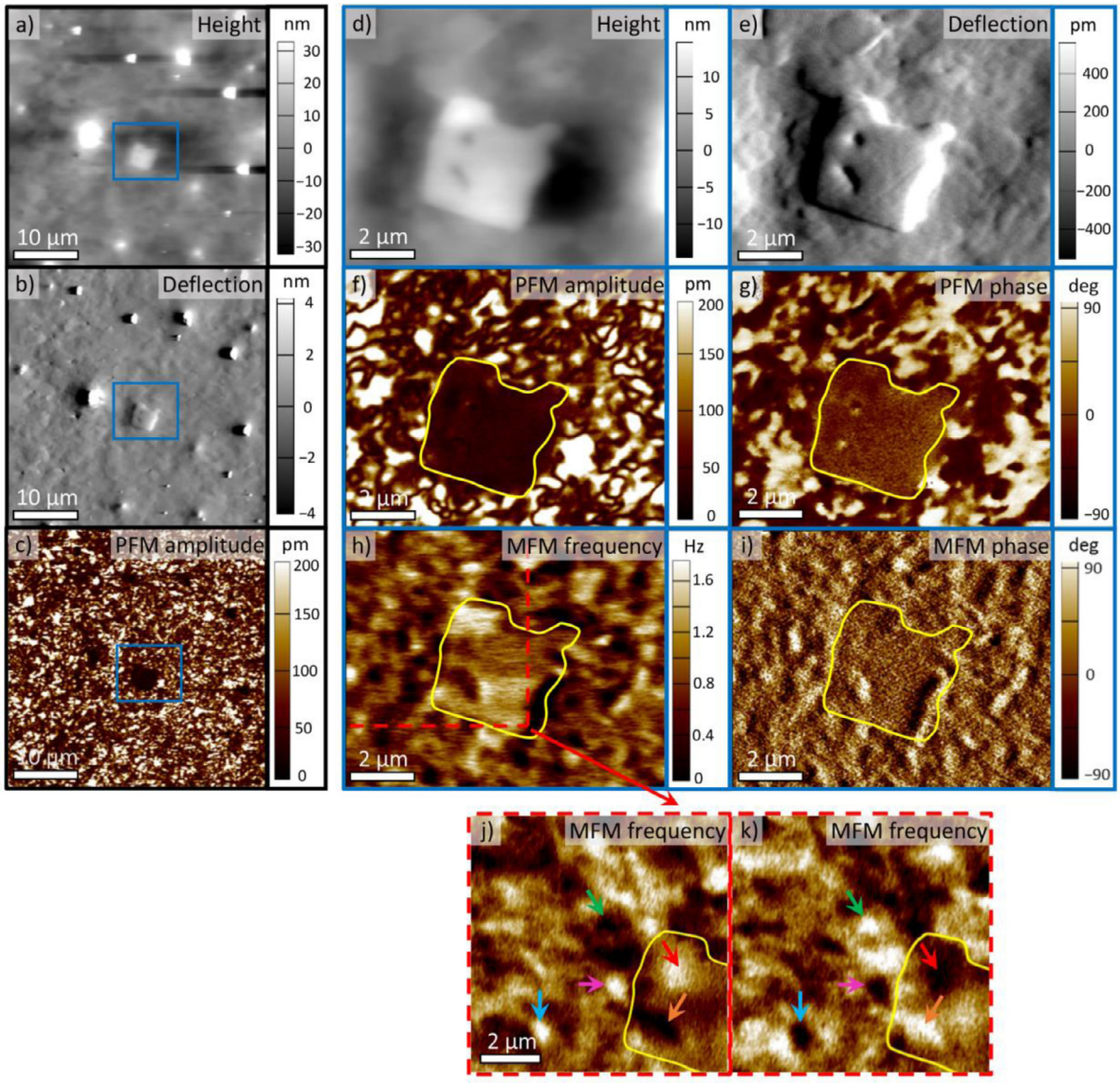


**Fig. 3.** 40 × 40 µm AFM topography a) height, b) deflection and c) PFM amplitude images of $B_{0.88}Gd_{0.12}FeO_3$ ceramic surface. The blue square highlights a region with an of Fe-rich inclusion magnified in panels d) to i), where the yellow line traces the perimeter of the Fe-rich phase. d) and e) show AFM height and deflection. f) and g) show images from PFM amplitude and phase measurement modes. h) and i) show images from MFM frequency and phase signal. j) and k) show still higher magnification MFM frequency measurements performed with opposite polarity of the magnetic MFM tip. The five arrows highlight regions of opposite contrast in the perovskite matrix and in Fe-rich phase.

To confirm the magnetic domain structure in the material the measurement was repeated with opposite tip polarity (Fig. 3j and k). When employing this method, the pattern of bright and dark phases should reverse if the response is derived from the magnetic interaction between the tip and the sample. If the signal derives from sample topography or some other phenomenon, then the contrast should not reverse. The five arrows in Fig. 3j and 3k direct attention to five distinct regions in the perovskite matrix where the contrast is reversed with the tip polarity, providing strong evidence that the signal results from the magnetic properties of the sample and corresponds to the magnetic domain structure. The presence of both the piezoelectric (Fig. 3f) and magnetic signals (Fig. 3h), with spatial distributions correlating with the ferroelectric and ferromagnetic domains structures respectively, provides evidence of the intrinsic multiferroicity of the perovskite matrix in $Bi_{0.88}Gd_{0.12}FeO_3$. Meanwhile the secondary phase possesses a magnetic response but no piezoelectric response. The measurements clearly demonstrate that both the matrix and the secondary phase possess magnetic domains, and thus must both contribute to the macroscopic magnetic response of the material.

Bismuth ferrite ceramics modified with 12 mol% gadolinium possess a multiferroic rhombohedral *R*3*c* matrix phase with secondary phases scattered throughout the microstructure. The $Bi_{0.88}Gd_{0.12}FeO_3$ is ferromagnetic, with a coercive field of 8 kOe and remanent magnetization of 0.2 emu·g$^{-1}$, confirming that rare earth substitution breaks the antiferromagnetic ordering of the parent bismuth ferrite. Local PFM and MFM measurements show that the matrix possesses both ferroelectric/ferroelastic and ferromagnetic domain structures and is thus intrinsically multiferroic. Fe-rich secondary phases found in as sintered ceramics were not piezoelectric but weakly ferrimagnetic. Thermal excursions to 1000 °C significantly impacted the macroscopic magnetization and when considered together with the known $Bi^{3+}$ volatility and thermodynamic instability of $BiFeO_3$, show the significant impact that iron oxides can have on the magnetic properties. This work confirms the multiferroic potential of rare earth modified bismuth fer-

rite ceramics and suggests that further studies should be directed towards the minimization of the magnetic secondary phases during processing and thermal cycling.

## Declaration of Competing Interest

None.

## Acknowledgements

The authors thank the financial support from the Slovenian Research Agency (project *Multicaloric cooling* J2–9253, young researcher projects PR-07594 and PR-08977 and research core funding No. P2–0105). center of Excellence NAMASTE is acknowledged for access to the AFM equipment. O.A.C. acknowledges JECS Trust (Contract 2019296) for financial support and Prof. Liliana Mitoseriu from University "A.I Cuza", Iasi, Romania for the kind help and guidance. JW also acknowledges funding from NTNU.

## Supplementary materials

Supplementary material associated with this article can be found, in the online version, at doi:10.1016/j.scriptamat.2020.07.045.

## References

[1] R. Ramesh, N.A. Spaldin, Nat. Mater. 6 (2007) 21.
[2] G. Catalan, J.F. Scott, Adv. Mater. 21 (2009) 2463.
[3] J.M. Moreau, C. Michel, R. Gerson, W.J. James, J. Phys. Chem. Solids 32 (1971) 1315.
[4] I. Sosnowska, T.P. Neumaier, E. Steichele, J. Phys. C: Sol. Stat. Phys. 15 (1982) 4835.
[5] D. Lebeugle, D. Colson, A. Forget, M. Viret, Appl. Phys. Lett. 91 (2007) 022907.
[6] J. Wang, J.B. Neaton, H. Zheng, V. Nagarajan, S.B. Ogale, B. Liu, D. viehland, V. Vaithyanathan, D.G. Schlom, U.V. Waghmare, N.A. Spaldin, K.M. Rabe, M. Wuttig, R. Ramesh, Science 299 (2003) 1719.
[7] G.L. Yuan, S.W. Or, Y.P. Wang, Z.G. Liu, J.M. Liu, Solid State Commun. 138 (2006) 76.
[8] M. Kumar, S. Shankar, O.P. Thakur, A. k. Ghosh, J. Mater Sci: Mater. Electron. 26 (2015) 1427.
[9] T. Murtaza, J. Ali, M.S. Khan, K. Asokan, J. Mater. Sci: Mater. Electron. 29 (2018) 2110.
[10] G.L. Yuan, S.W. Or, J. Appl. Phys. 100 (2006) 024109.
[11] I.I. Makoed, A.F. Revinskii, Phys. Solid State 57 (2015) 1787.
[12] D. Kan, L. Palova, V. Anbusathaiah, C.J. Cheng, S. Fujino, V. Nagarajan, K.M. Rabe, I. Takeuchi, Adv. Funct. Mater. 20 (2010) 1108.
[13] A. Kumar, A. Kumar, S. Saha, H. Basumatary, R. Ranjan, Appl. Phys. Lett. 114 (2019) 022902.
[14] M. Valant, A.-K. Axelsson, N. Alford, Chem. Mater. 22 (2007) 5431.
[15] S.M. Selbach, M.A. Einarsrud, T. Grande, Chem. Mater. 21 (2009) 169.
[16] J. Walker, P. Bryant, V. Kurusingal, C. Sorrell, D. Kuscer, G. Drazic, A. Bencan, V. Nagarajan, T. Rojac, Acta Mater. 83 (2015) 149.
[17] U. Hartmann, Annu. Rev. Mater. Sci. 29 (1999) 53.
[18] J. Walker, H. Ursic, A. Bencan, B. Malic, H. Simons, I. Reaney, G. Viola, V. Nagarajan, T. Rojac, J. Mater. Chem. C. 16 (2016) 7859.
[19] T. Rojac, A. Bencan, B. Malic, G. Tutuncu, J.L. Jones, J.E. Daniels, D. Damjanovic, J. Amer. Ceram. Soc. 97 (2014) 1993.
[20] A.M. Kadomtseva, Y.F. Popov, A.P. Payatakov, G.P. Vorob'ev, A.K. Zvezdin, D. Vieland, Phase Trans. 79 (2006) 1019.
[21] V.A. Khomchenko, D.A. Kiselev, I.K. Bdikin, V.V. Shvartsman, P. Borisov, W. Kleemann, J.M. Vieira, A.L. Kholkin, Appl. Phys. Lett. 93 (2008) 262905.
[22] N. Shamir, E. Gurewitz, H. Shaked, Acta Cryst. A. 34 (1978) 662.
[23] J. Walker, B. Budic, P. Bryant, V. Kurusingal, C.C. Sorrell, A. Bencan, T. Rojac, IEEE Transactions on Ultrasonics, Ferroelectrics and Frequency Control 62 (2015) 83.
[24] D. Giuntini, E. Torresani, K.T. Chan, M. Blankenburg, L. Saviot, B. Bor, B. Domenech, M. Shachar, M. Muller, E.A. Olevsky, J.E. Garay, G.A. Schneider, Nanoscale Adv. 1 (2019) 3139–3150.
[25] T. Zhao, A. Scholl, F. Zavaliche, K. Lee, M. Barry, A. Doran, M.P. Cruz, Y.H. Chu, C. Ederer, N.A. Spaldin, R.R. Das, D.M. Kim, S.H. Baek, C.B. Eom, R. Ramesh, Nat. Mater. 5 (2006) 823.
[26] D. Chen, X. Gao, J.-.M. Liu, MRS Commun. 6 (2016) 330.